Computational and Theoretical Chemistry 1228 (2023) 114258

Contents lists available at ScienceDirect

Computational and Theoretical Chemistry

journal homepage: www.elsevier.com/locate/comptc

Uncovering the remarkable electrochemical performance of B_2N_2 monolayer as a promising candidate for Mg-ion batteries

Chou-Yi Hsu [a], Ayat Hussein Adhab [b], Daha Thabit [c], Shelesh Krishna Saraswat [d,*], Sura Mohammad Mohealdeen [e], Abdelmajeed Adam Lagum [f], Alaa M. Al-Ma'abreh [g], Samer Alawideh [g], Saroj Sharma [h,*]

[a] Department of Pharmacy, Chia Nan University of Pharmacy and Science, Tainan City, 71710, Taiwan
[b] Department of Pharmacy, Al-Zahrawi University College, Karbala, Iraq
[c] Medical technical college, Al-Farahidi University, Iraq
[d] Department of Electronics and Communication Engineering, GLA University, Mathura-281406, India
[e] Department of Radiology & Sonar Techniques, Al-Noor University College, Nineveh, Iraq
[f] Department of Civil Engineering, Faculty of Engineering, Isra University, P.O. Box 22, Amman, 11622, Jordan
[g] Department of Chemistry, Faculty of Science, Isra University, P.O. Box 22, Amman, 11622, Jordan
[h] Department of Chemistry, Govt. Nagarjuna PG College of Science, Raipur, 492010, India

ARTICLE INFO

Keywords:
Mg-ion battery
Specific capacity
Diffusion barrier
o-B_2N_2 monolayer

ABSTRACT

Nowadays, owing to their potential applications in next-generation self-powered electronic devices, such as energy-harvesting smart garments from body movements and roll-up displays, electrochemical energy storages are enjoying considerable interest. Nonetheless, the development of such technologies has been hindered due to the rarity of high-efficacy electrodes with specific electrochemical performance. Amongst prospective electrodes, researchers have investigated 2D flexible and lightweight materials which have unique physiochemical attributes such as high conductance, high surface metal diffusivity, a hydrophilic surface and mechanical strength. Within this piece of research, a 2D orthorhombic di-boron di-nitride monolayer (o-B_2N_2ML), which is a boron nitride allotrope, was investigated. Moreover, several determining electronic chemical factors were investigated, such as theoretical capacity, equilibrium voltage and binding strength. Interestingly, the Mg-ion battery had a specific capacity of up to 1125 mAh.g^{-1}. Also, the diffusion of Mg-ions was accelerated due to the presence of a o-B_2N_2 ring with a diffusion barrier (DB) of 0.26 eV. The low OCV and the low DB of the o-B_2N_2ML demonstrate that it can be used for practical purposes with long service life and fast rates of charge and discharge. The results also indicated the possible use of the o-B_2N_2ML as an anode material with high efficiency in MIBs.

1. Introduction

Recent years have witnessed the tremendous impact of energy storage systems, such as large power grids, hybrid vehicles and portable devices, on the daily lives of people [1–8]. Owing to their light weight, long cycle life and high energy storage efficiency, the energy storage market has been dominated by rechargeable lithium-ion batteries (LIBs) [9–15]. Nonetheless, the scarcity of lithium, poor safety and low theoretical specific capacities have limited the development and commercialization of LIBs [16–21]. As a solution, researchers have investigated alternative batteries which do not use lithium as the anode material for accommodating high energy. The newly introduced substitutes for LIBs, such as potassium-ion batteries (KIBs) and sodium-ion batteries (NIBs), are eco-friendlier and greener. It should be mentioned that divalent ion-based batteries (such as Zn^{2+}, Ca^{2+} or Mg^{2+}) are more suitable than monovalent ion-based batteries (such as K^+ and Na^+) in terms of their capacity since they can transfer two electrons [22–30]. Herein, calcium-ion batteries (CIBs), MIBs, KIBs and NIBs are collectively called non-lithium-ion batteries (NLIBs) [31–33]. These batteries have abundant raw materials on earth and their purification is easy. Nevertheless, the radius of Ca, Mg, K and Na ions is larger than the radius of Li ion and they have a heavier mass. This raises questions regarding the usability of traditional electrodes [34–37]. According to the literature, electrolyte and electrode materials (EMs) are considered important in determining

* Corresponding authors.
E-mail addresses: sheleshkrishnasaraswat@gmail.com (S. Krishna Saraswat), saroj.sharma.chem@gmail.com (S. Sharma).

https://doi.org/10.1016/j.comptc.2023.114258
Received 2 July 2023; Received in revised form 20 July 2023; Accepted 23 July 2023
Available online 24 July 2023

the electronic and chemical performance of NLIBs unlike LIBs [38]. Until now, researchers have investigated and found new materials, such as Prussian blue frameworks [39], layered TMO [40] and olivine $FePO_4$ [41] with superior cycling performance, high capacity and large interstitial spaces, which can be used as potential cathode materials. Despite a large body of research on developing cathode materials, little research can be found on developing anode materials, which is limited to V_A and VI_A group element compounds and C-based materials [42,43]. Unfortunately, anode materials which can be used effectively in LIBs cannot be used in NLIBs. For example, the electrochemical activity of graphite for non-Li ions, which is commonly used in commercial LIBs, is low [44]. Therefore, developing anode materials which have high conductance, large capacity, fast intercalation/deintercalation and high reversibility can widen the applications of NLIBs. Combining other 2D layered materials with graphene for forming 2D heterostructures is another workable solution. The electrochemical stability, conductivity and conductance of heterostructure-based electrodes are high. However, ion transfer is limited in these electrodes due to the tight filling between layers [45].

A lot of pieces of research have been done on the hexagonal boron nitride (h-BN) as an encouraging 2D material because of its unique properties such as a wide bandgap (6 eV). However, the indirect wide bandgap of the h-BN has also limited its performance as a anode material [46]. Since anode materials must possess high conductance [3], the weak interactions between the surface of the h-BN and different metals along with the insufficient adhesion of Li for the conversion of indirect wide bandgap into a metallic nature have further limited the application of the h-BN for energy storage purposes [47,48]. In 2003, Demirci et al. [49] proposed a o-B_2N_2 monolayer (o-B_2N_2ML), which is a 2D polygraph of Gr-like BN through density functional theory (DFT). which had an orthorhombic structure. The results demonstrated that the o-B_2N_2ML had dynamic and mechanical stability. Furthermore, based on the Ab-initio molecular dynamic calculations, geometrical structure integrity of the o-B_2N_2ML was as high as 1000 K for 10 ps [50]. The newly proposed o-B_2N_2ML, which exhibited a direct narrow bandgap (0.64 eV), can have a great prospective in the future in hydrogen storages, rechargeable batteries, photovoltaics and energy storage and conversion devices [49]. More importantly, the o-B_2N_2ML is capable of reaching a very high theoretical specific capacity (TSC) for batteries since both nitride and boron are extremely light elements whose molecular weights are approximately 14.0067 a.u and 10.811 a.u [50].

Within this piece of research, the application of the o-B_2N_2ML as an EM in MIBs was investigated for the first time through DFT calculations. First, the electronic attributes and the structural optimization of the o-B_2N_2ML were thoroughly investigated. Next, DFT and DFT-D3 were used to calculate the binding strength of Mg at potential sites on the surface of the o-B_2N_2ML. Using a universal optimization procedure based on DFT-D3 computations, we also investigated the theoretical capacity and equilibrium voltage. Afterwards, we computed the deformation charge density and charge transport following the adhesion of an Mg atom, and we later computed the ionic diffusion during the adhesion of Mg on the o-B_2N_2ML. By comparing the newly proposed o-B_2N_2ML within this study to other available materials, it was revealed that the B_2N_2ML has a dramatically lower ionic mobility and higher TSC as an EMs.

2. Computational details

The basis set 6-31G (d) and the functional B3LYP were used to perform the electronic analyses, energy estimations and structural optimizations. For the sake of predicting weak interactions, the Grimme's "D3" term was applied [51]. According to previous studies, B3LYP can precisely describe the structural-electronic attributes of nanomaterials [52–56]. The calculations were all performed through the GAMESS program [57]. The Bader charge analysis (BCA) was undertaken for analyzing the charge transported between the o-B_2N_2ML and the Mg ions [58]. We also computed the diffusion paths of Mg ions, and the NEB method [59] was adopted for estimating the diffusion barrier (hereafter DB) energies. Additionally, the adhesion energy of the Mg atom onto the o-B_2N_2ML substrates was estimated as below [60]:

$$E_{ad} = \frac{(E_{Mg@o-B_2N_2} - (E_{o-B_2N_2} + xE_{Mg}))}{x} + E_{BSSE} \quad (1)$$

Herein, we simplified the charging and discharging process of the o-B_2N_2 Ml as a half-cell reaction as follows:

$$xMg^{+} + xe^{-} + o - B_2N_2 \leftrightarrow Mg_x@o - B_2N_2 \quad (2)$$

The formula below can be obtained for computing the open-circuit voltage using the reaction model above [60]:

$$VOCV = \frac{(E_{Mg@o-B_2N_2} - (E_{o-B_2N_2} + xE_{Mg}))}{xe} \quad (3)$$

here, x shows the number of Mg atoms, E_{Mg} is the energy of a Mg atom in the bulk system, Eo_{-B2N2} is the energy of the pure o-B_2N_2 ML and $E_{Mg@o-B2N2}$ is the total energy of Mg adhered onto the o-B_2N_2ML. The negative adhesion energy values indicated the adhesion the Mg atoms onto the pure o-B_2N_2ML. We computed the maximum storage capacity as follows [16,17,61]:

$$C = \frac{x_{max}F}{M} \quad (4)$$

here, F signifies the Faraday constant (26.81 A h mol^{-1}), x_{max} shows the maximum number of Mg atoms adhered, and M shows the atomic mass.

3. Results and discussions

3.1. Electronic and structural attributes

There is still a growing interest in designing and identifying modern and high-efficacy 2D materials for batteries despite the tremendous advances made. Thus far, little research has been done on the electronic conductance of negative EMs, which is one of the important screening factors in improving their charge and discharge performance [62–64]. One of the prerequisites for the transfer of electrons is high conductance for a negative EMs. An ideal anode material consists of highly conductive metallic conductors or semiconductors. However, this aspect should be further investigated through computational and theoretical approaches as studies on t insulating materials as the electrodes of batteries increase. Thanks to its wide applications, one of the commonly investigated 2D material with a Gr-like structure is the h-BN (see Figure 1 (a, b)) [65]. Nonetheless, the limited attributes and the wide bandgap of h-BN have limited its applicability as a negative EM in rechargeable batteries [48]. Hence, an alternative structure of BN with stability should be explored which is formed by rearranging the N and B atoms with enhanced conductance and optimal electrochemical attributes. The o-B_2N_2ML, which was first introduced by Dimiciri et al. [49], is a novel 2D material which has the same planar honeycomb crystalline structure as h-BN and Gr. The top-viewed optimized structures of h-BN and o-B_2N_2ML are shown in Fig. 1(b). 4 atoms made of cyclical B–B, B–N, and N—N bonds form theo-B_2N_2ML primitive cell. The length of B–B was 1.73 Å, that of B–N was1.44 Å, and that of N—N was 1.44 Å, and the optimized Bravais vectors of o-B_2N_2ML were a = 4.57 Å and b = 2.46 Å, similar to values obtained in the literature [49].

The valence electron localization function was calculated for the sake of characterizing the electron localizations in the interstitial spaces and understanding the chemical bonds of the o-B_2N_2ML. The electrons were mainly localized in the N—N, B–N and B–B bonds in comparison with the hollow sites with zero electron localization. The findings demonstrated that there were covalent bonding properties on the surface of the o-B_2N_2ML.The BCA was undertaken for investigating the net charge of B and N atoms, which was approximately + 0.92 |e| and − 0.92 |e|, respectively. The electronic band structures and the related

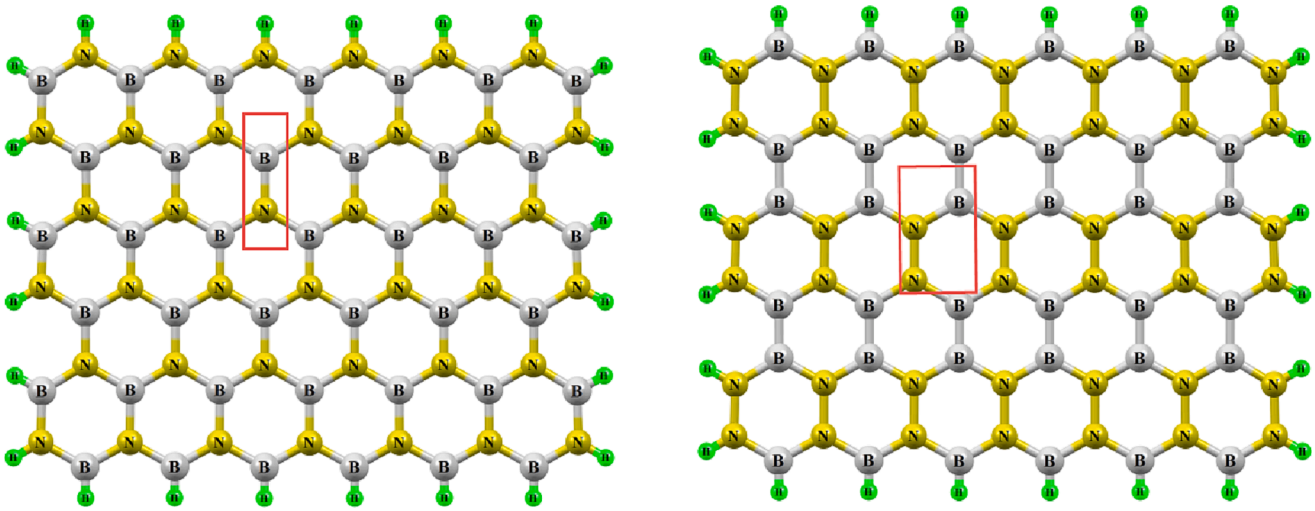

Fig. 1. Top view of a free-standing (a) h-BN and (b) o-B_2N_2 monolayers.

DOS were computed for both h-BN and o-B_2N_2ML. Based on the results, the o-B_2N_2 ML had a semiconducting property with a band gap of 0.75 eV, which was less than that of the h-BN (3.46 eV).

3.2. The adhesion of a single Mg atom onto o-B_2N_2ML

One of the prerequisites for negative EMs in MIBs is the relatively high binding strength of Mg atoms. So, DFT-D3 was adopted to calculate the binding strength of a single Mg atom at potential sites on theo-B_2N_2ML. For the sake of inhibiting the interaction between adjacent Mg ions on the o-B_2N_2ML, we large -B_2N_2ML with 10*15 Å was used during the process of Mg intercalation. We took into account 7 sites at the outset because the o-B_2N_2Ml had a D2h symmetry. They were further classified into 3 categories, namely T (top), B (Bridge), and H (hollow) (see Figure 2 (a)). H contained H-1 and H-2 which were over the hollow site of B_4N_2- and B_2N_4-Hexagons, respectively. T contained *T*-B and *T*-*N* located atop of B and N atoms with regard to the crystal symmetry. B contained B-1 (between B–B), B-2 (between N—N), and B-3 (between B–N).

As the binding strength becomes more negative, the stability of the binding configuration becomes more, which indicated that the Mg-atoms have a scattering distribution rather than clustering, so the problem due to the formation of metal clusters or dendrites or metal-clusters during the charging and discharging processes can be avoided. The binding energy of the Mg atom at H1 and H2 was the lowest, with remaining sites deviating to H2 or H1. The work function, charge transport and the binding heights for the first sites with most stability computed using DFT and DFT-D3 are summarized in Table 1. As could be seen, the binding strength of H1 was the lowest (–0.953 eV). The fully optimized geometry of Mg atom at H1 is shown in Fig. 2(b))). The binding strength obtained is higher than the one reported for other materials [47,48,66]. This revealed that the charging process was very fast and the binding interaction between the Mg atom and the orthorhombic was more extensive compared to the weak interaction of metal ions in the h-BN [47]. Furthermore, the results revealed that the Mg atoms were uniformly spread on the o-B_2N_2ML during the intercalation rather than forming dendrites, which ensured high stability, reversibility and safety for next-generation Mg^{2+}-based batteries.

Table 1
E_{ad} using DFT and DFT-D3, binding height, charge transfer Q (|e|), and work function of Mg adsorbed on the most favorable binding site.

Site	$E_{ad\text{-}DFT}$ (eV)	$E_{ad\text{-}DFT\text{-}D3}$ (eV)	Q (e)	E_b (eV)
H1	−0.953	−1.013	0.512	0.26
H2	−0.869	−0.939	0.207	0.57

3.3. OCV and theoretical storage capacity (TSC)

Through the step-wise insertion of the Mg ion into the both sides of the o-B_2N_2, the OCV and the record-high TSC were examined to investigate the electronic and chemical performance of o-B_2N_2 in MIBs. First, since the energetic stability of sites H1 and H2 was more, we inserted the Mg atoms at site H1 on both sides of o-B_2N_2 until reaching a recovery, which formed the first Mg layer. Next, we located the Mg at H2, which formed the second Mg layer, so a series of intermediate configurations were considered with the chemical formula $Mg_x@B_2N_2$ (x = 0.5, 1.0, 1.5, 2.0, 2.5, 3.0). During the charging process, the binding energies of all configurations remained negative, which prevented dendrites from forming. So, o-B_2N_2 as an anode for MIBs is capable of storing $Mg@B_2N_2$. Hence, the theoretical specific Mg storage capacity on B_2N_2 was approximately 1125 mAh/g. It should be also mentioned that the Mg storage capacity of the o-B_2N_2ML was dramatically high. A review of the recent literature also demonstrated the Mg-storage capacity of the B_2N_2 is dramatically more than that of reported 2D materials [67–70].

Potential voltage is another important factor in assessing the efficiency of MIBs. In Fig. 3, the black line demonstrated that OCV changed according to the Mg concentration. As can be seen, the OCV values were positive, which demonstrated that the o-B_2N_2ML can be used negative electrode in MIBs. Moreover, after increasing the concentration of Mg ions, there was an increase in the OCV via the insertion of 4 Mg potential plateaus with an average voltage of around 0.404 V vs. Mg^{2+}/Mg. In order to obtain maximum power density during the charging and discharging processes, a moderate average voltage like this can be favourable, which can enhance the stability of electrodes by preventing dendrites from forming. Therefore, it is possible to utilize o-B_2N_2ML as an anode material in MIBs.

3.4. Diffusion kinetics and charge transport

The performance of negative EMs, particularly during the charging and discharging processes is a crucial factor in developing Mg-based RBs with high performance, which is determined by the kinetic property of electron transport. Hence, we investigated the difference in the charge density of Mg atoms adhered the optimal site on the o-B_2N_2ML. The accumulation and depletion of charge for both systems shown as three-dimensional isosurface distributed charge density plots are shown in Figure 4. As could be seen, the area with charge accumulation (yellow color) was located inside the Mg atom and the o-B_2N_2ML surface, and

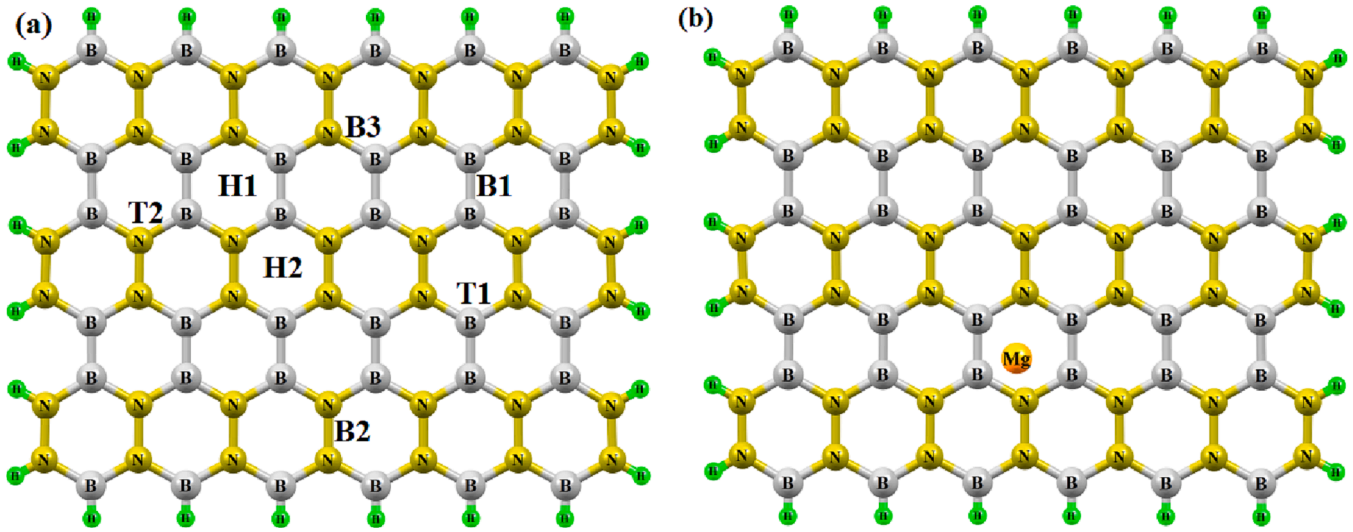

Fig. 2. (a) The suitable binding sites for Mg on the free-standing o-B_2N_2 monolayer (T2/T1 refers to the binding sites at the top of N/B atoms; H1 and H2 denote the hollow-sites of the hexagonal B_4N_2-ring and B_2N_4-ring, respectively; B1, B2, and B3 denotes the binding sites at the B–B, N—N, and B–N bridges, respectively). (b) The top views of the most stable optimized configuration of single Mg atom adsorbed on the o-B_2N_2 monolayer.

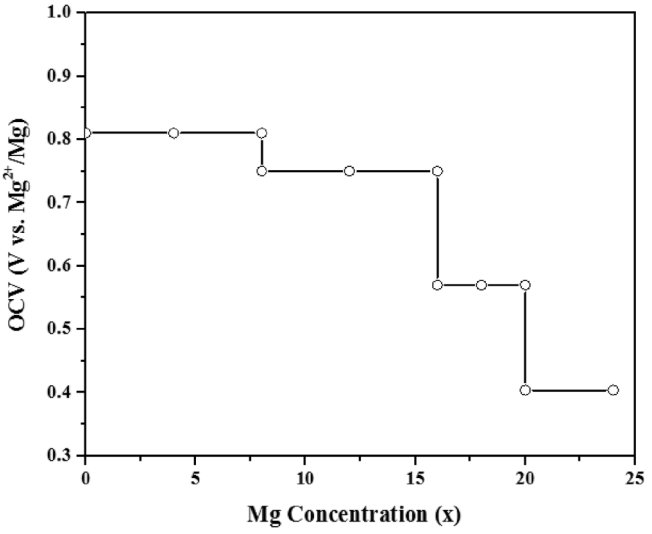

Fig. 3. The voltage profiles (V) with average binding strength (eV) as a function of the Mg concentration (x).

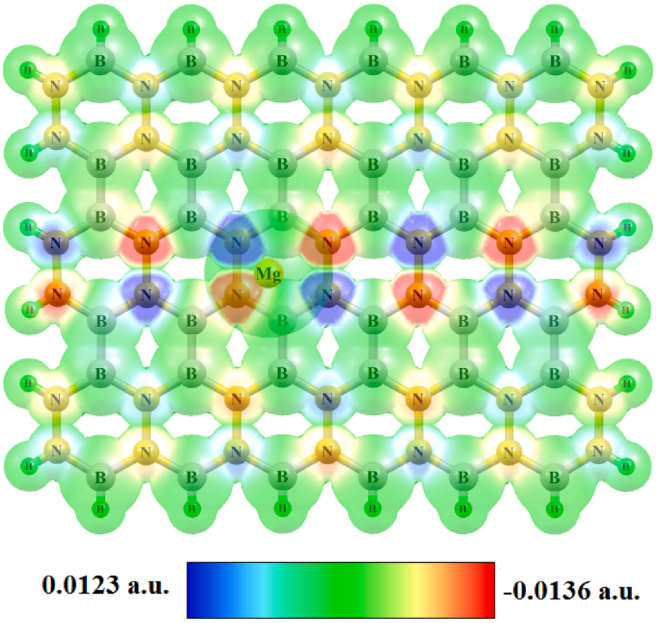

Fig.4. Side view of difference charge density (Δρ) for Mg-atom adsorbed at the most stable binding site (H1) on o-B_2N_2 surface.

the area with charge depletion (light blue color) surrounded the Mg atom, showing that the Mg atom donate charge to the o-B_2N_2ML, which caused B and N atoms to be more electronegative than the Mg atoms. Additionally, the charge transport was determined by performing the BCA, results were provided in Table 1. As could be seen, each Mg atom lost about a charge of around 0.512 |e|.

Another important factor affecting the electronic and chemical performance of batteries, particularly high charging and discharging processes, is the diffusion of Mg ions, which was investigated to further investigate the performance of the o-B_2N_2ML [63]. Hence, we computed the dilute diffusion paths of Mg ions and the related MEP by performing the NEB method. Fig. 5 shows the top-view optimized 3 diffusion pathways (A, B, C) and the related MEP. The paths considered included the migration of an Mg ion along the Zigzag (direction a, pathway A), armchair (direction b, pathway B), and pathway C (atop site H2) on the surface of the o-B_2N_2ML. In Pathway A, the Mg ion was diffused along direction b, and perpendicular to N—N and B–B bonds with an EB of approximately 0.26 eV. However, in Path B, the Mg ion diffused from H1 (with the most stability and BE) to the closest site H1 parallel to N—N and B–B bonds along direction a. As could be seen, the Mg ion had to surmount an EB of 0.59 eV. In addition, in Path C, the Mg ion was scattered atop H2 with MEP of 1.02 eV. The computed EB values were in line with binding energies provided in Table 1, the diffusion barrier of the Mg ion in Pathway A exhibited the lowest energy profile in comparison with Pathway B and Pathway C. The results revealed the possibility of using the o-B_2N_2ML as an EM in future batteries.

4. Conclusion

The potential use of the o-B_2N_2ML as an EM in MIBs was investigated for the first time by considering important factors through DFT computations. We thoroughly examined the ionic-mobility, kinetics and the binding strength of Mg intercalation. Based on the results, the Mg atoms were inserted into the structure of the o-B_2NML without forming clusters

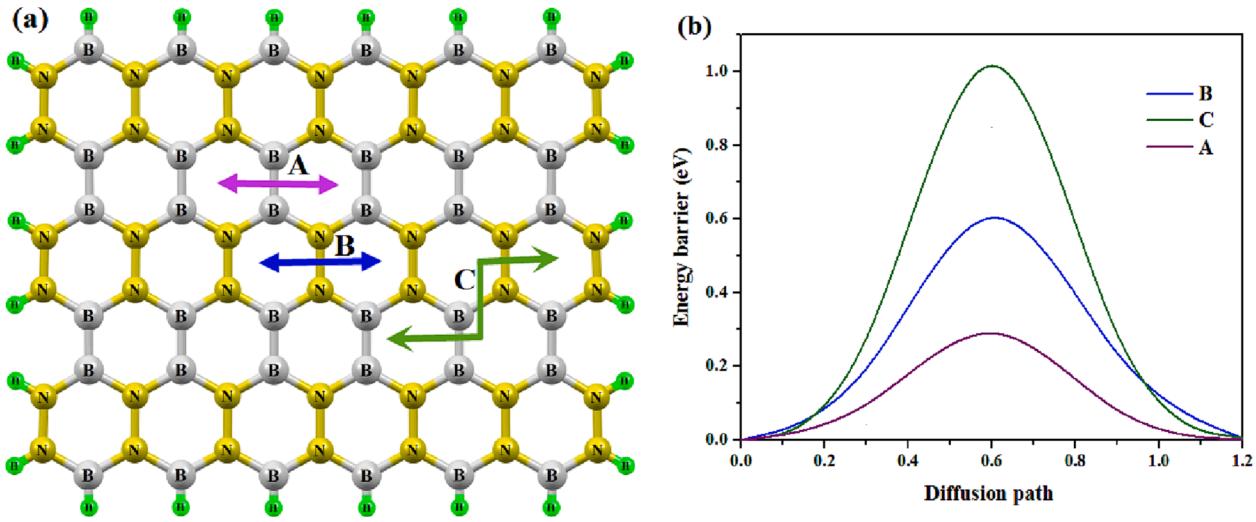

Fig.5. (a) The top view of the full optimized three various Mg-ion diffusion pathways (A, B, and C). (b) The corresponding minimum energy barriers for Mg-ion along the three pathways.

and they were adhered on the hollow site on the surface of the o-B_2NML and the binding strength was around − 1.013 eV. A TSC of around 1125 mAh/g was obtained thanks to the high Mg storage capacity on both sides of the o-B_2NML, which was higher than those of other materials for Mg storage. Moreover, a relatively low OCV of around 0.404 eV can be advantageous for high-performance MIBs. Owing to the above-mentioned electrochemical attributes, the o-B_2N_2ML is expected to have widespread application as an EM in MIBs. Finally, the current study can provide guidelines for both experimental and theoretical studies investigating the application of 2D anode materials.

CRediT authorship contribution statement

Chou-Yi Hsu: Conceptualization, Methodology, Software, Data curation, Writing – original draft. **Ayat Hussein Adhab:** Conceptualization, Methodology, Software, Data curation, Writing – original draft. **Daha Thabit:** Conceptualization, Methodology, Software, Data curation, Writing – original draft. **Shelesh Krishna Saraswat:** Conceptualization, Methodology, Software, Data curation, Writing – original draft. **Sura Mohammad Mohealdeen:** Visualization, Investigation, Methodology. **Abdelmajeed Adam Lagum:** Visualization, Investigation, Methodology. **Alaa M. Al-Ma'abreh:** Software, Validation, Data curation, Writing – review & editing. **Samer Alawideh:** Software, Validation, Data curation, Writing – review & editing. **Saroj Sharma:** Software, Validation, Data curation, Writing – review & editing.

Declaration of Competing Interest

The authors declare that they have no known competing financial interests or personal relationships that could have appeared to influence the work reported in this paper.

Data availability

No data was used for the research described in the article.

References

[1] C. Tang, M. Zhang, K. Zhang, J. Gong, Promising anode material BN/VS2 heterostructure for the Li-ion battery: The first-principles study, Applied Surface Science 564 (2021) 150468.
[2] F. Ling, X. Liu, L. Li, X. Zhou, X. Tang, Y. Li, C. Jing, Y. Wang, G. Xiang, S. Jiang, Novel CuTe monolayer as promising anode material for Na-ion batteries: A theoretical study, Applied Surface Science 573 (2022) 151550.
[3] X. Zhao, P. Wang, E. Lv, C. Wu, K. Ma, Z. Gao, I.D. Gates, W. Yang, Screening MXenes for novel anode material of lithium-ion batteries with high capacity and stability: A DFT calculation, Applied Surface Science 569 (2021) 151050.
[4] X. He, A. Tang, Y. Li, Y. Zhang, W. Chen, S. Huang, Theoretical studies of SiC van der Waals heterostructures as anodes of Li-ion batteries, Applied Surface Science 563 (2021) 150269.
[5] Y. Wang, M. Zhou, L.-C. Xu, W. Zhao, R. Li, Z. Yang, R. Liu, X. Li, Achieving superior high-capacity batteries with the lightest Ti2C MXene anode by first-principles calculations: Overarching role of S-functionate (Ti 2CS2) and multivalent cations carrier, Journal of Power Sources 451 (2020) 227791.
[6] C. Qiu, L. Jiang, Y. Gao, L. Sheng, Effects of oxygen-containing functional groups on carbon materials in supercapacitors: A review, Materials & Design 111952 (2023).
[7] Q. Liu, Q. Chen, Y. Tang, H.-M. Cheng, Interfacial modification electrode/solid-electrolyte engineering, and monolithic construction of solid-state batteries, Electrochemical Energy Reviews 6 (2023) 15.
[8] C. Lu, C. Xu, W. Sun, R. Ren, J. Qiao, Z. Wang, K. Sun, G. Pan, Y. Cao, Enhancing catalytic activity of CO2 electrolysis by building efficient and durable heterostructure for solid oxide electrolysis cell cathode, Journal of Power Sources 574 (2023) 233134.
[9] N. Khossossi, A. Banerjee, I. Essaoudi, A. Ainane, P. Jena, R. Ahuja, Thermodynamics and kinetics of 2D g-GeC monolayer as an anode materials for Li/Na-ion batteries, Journal of Power Sources 485 (2021) 229318.
[10] X. Zhang, W. Meng, T. He, L. Jin, X. Dai, G. Liu, Mn2C monolayer: A superior anode material offering good conductivity, high storage capacity and ultrafast ion diffusion for Li-ion and Na-ion batteries, Applied Surface Science 503 (2020) 144091.
[11] S. Qi, F. Li, J. Wang, Y. Qu, Y. Yang, W. Li, M. Zhao, Prediction of a flexible anode material for Li/Na ion batteries: Phosphorous carbide monolayer (α-PC), Carbon 141 (2019) 444–450.
[12] C. Xiao, X. Tang, J. Peng, Y. Ding, Graphene-like BSi as a promising anode material for Li-and Mg-ion batteries: A first principle study, Applied Surface Science 563 (2021) 150278.
[13] Y. Du, Y. Xie, X. Liu, H. Jiang, F. Wu, H. Wu, Y. Mei, D. Xie, In-situ formed phosphorus modified gel polymer electrolyte with good flame retardancy and cycling stability for rechargeable lithium batteries, ACS Sustainable Chemistry & Engineering 11 (2023) 4498–4508.
[14] X. Cai, Z. Shadike, X. Cai, X. Li, L. Luo, L. An, J. Yin, G. Wei, F. Yang, S. Shen, Membrane electrode assembly design for lithium-mediated electrochemical nitrogen reduction, Energy & Environmental Science (2023).
[15] R. Ren, F. Lai, X. Lang, L. Li, C. Yao, K. Cai, Efficient sulfur host based on Sn doping to construct Fe2O3 nanospheres with high active interface structure for lithium-sulfur batteries, Applied Surface Science 613 (2023) 156003.
[16] C. Zhang, M. Yu, G. Anderson, R.R. Dharmasena, G. Sumanasekera, The prospects of phosphorene as an anode material for high-performance lithium-ion batteries: A fundamental study, Nanotechnology 28 (2017) 075401.
[17] C. Li, L. He, X. Li, J. Luo, X. Zhu, Z. Chen, M. Xu, Low in-plane atomic density phosphorene anodes for lithium-/sodium-ion batteries, Journal of Materials Chemistry C 9 (2021) 6802–6814.
[18] J. Wu, J. Yu, J. Liu, J. Cui, S. Yao, M.-I.-U. Haq, N. Mubarak, A. Susca, F. Ciucci, J.-K. Kim, MoSe2 nanosheets embedded in nitrogen/phosphorus co-doped carbon/graphene composite anodes for ultrafast sodium storage, Journal of Power Sources 476 (2020) 228660.
[19] J. Xie, X. Wei, X. Bo, P. Zhang, P. Chen, W. Hao, M. Yuan, State of charge estimation of lithium-ion battery based on extended Kalman filter algorithm, Frontiers in Energy Research 11 (2023).

[20] W. Hao, J. Xie, Reducing diffusion-induced stress of bilayer electrode system by introducing pre-strain in lithium-ion battery, Journal of Electrochemical Energy Conversion and Storage 18 (2021) 020909.
[21] J. Lu, Z. Wang, Q. Zhang, C. Sun, Y. Zhou, S. Wang, X. Qiu, S. Xu, R. Chen, T. Wei, The effects of amino groups and open metal sites of MOFs on polymer-based electrolytes for all-solid-state lithium metal batteries, Chinese Journal of Chemical Engineering (2023).
[22] H. Kang, Y. Liu, K. Cao, Y. Zhao, L. Jiao, Y. Wang, H. Yuan, Update on anode materials for Na-ion batteries, Journal of Materials Chemistry A 3 (2015) 17899–17913.
[23] S. Gurses, F. Ersan, Sodium adsorption, diffusion and coverage on two-dimensional GeP3, Sci. Acad. 1 (2020) 1–10.
[24] H. Wang, Y. Chen, H. Yu, W. Liu, G. Kuang, L. Mei, Z. Wu, W. Wei, X. Ji, B. Qu, A multifunctional artificial interphase with fluorine-doped amorphous carbon layer for ultra-stable Zn anode, Advanced Functional Materials 32 (2022) 2205600.
[25] X. Zhang, Y. Tang, F. Zhang, C.S. Lee, A novel aluminum–graphite dual-ion battery, Advanced energy materials 6 (2016) 1502588.
[26] M. Wang, C. Jiang, S. Zhang, X. Song, Y. Tang, H.-M. Cheng, Reversible calcium alloying enables a practical room-temperature rechargeable calcium-ion battery with a high discharge voltage, Nature chemistry 10 (2018) 667–672.
[27] S. Mu, Q. Liu, P. Kidkhunthod, X. Zhou, W. Wang, Y. Tang, Molecular grafting towards high-fraction active nanodots implanted in N-doped carbon for sodium dual-ion batteries, National science review 8 (2021) nwaa178.
[28] Y. Wei, B. Tang, X. Liang, F. Zhang, Y. Tang, Ultrahigh mass-loading integrated free-standing functional all-carbon positive electrode prepared using architecture tailoring strategy for high-energy-density dual ion battery, Advanced Materials 2302086 (2023).
[29] L. Li, S. Jia, Z. Cheng, C. Zhang, Improved Strategies for Separators in Zinc-Ion Batteries, ChemSusChem 16 (2023) e202202330.
[30] S. Du, H. Xie, J. Yin, Y. Sun, Q. Wang, H. Liu, W. Qi, C. Cai, G. Bi, D. Xiao, Giant hot electron thermalization via stacking of graphene layers, Carbon 203 (2023) 835–841.
[31] L. Sha, B.-B. Sui, P.-F. Wang, Z. Gong, Y.-H. Zhang, Y.-H. Wu, L.-N. Zhao, F.-N. Shi, Printing 3D mesh-like grooves on zinc surface to enhance the stability of aqueous zinc ion batteries, Journal of Colloid and Interface Science (2023).
[32] G. Huang, Q. Kong, W. Yao, Q. Wang, High proportion of active nitrogen-doped hard carbon based on mannich reaction as anode material for high-performance sodium-ion batteries, ChemSusChem 16 (2023) e202202070.
[33] Z. Huang, P. Luo, H. Zheng, Z. Lyu, X. Ma, Novel one-dimensional V3S4@ NC nanofibers for sodium-ion batteries, Journal of Physics and Chemistry of Solids 172 (2023) 111081.
[34] Y. Jing, J. Liu, Z. Zhou, J. Zhang, Y. Li, Metallic Nb2S2C monolayer: a promising two-dimensional anode material for metal-ion batteries, The Journal of Physical Chemistry C 123 (2019) 26803–26811.
[35] D. Spada, B. Albini, P. Galinetto, D. Versaci, C. Francia, S. Bodoardo, G. Bais, M. Bini, FeNb11O29, anode material for high-power lithium-ion batteries: Pseudocapacitance and symmetrisation unravelled with advanced electrochemical and in situ/operando techniques, Electrochimica Acta 393 (2021) 139077.
[36] Q. He, Z. Li, W. Xiao, C. Zhang, Y. Zhao, Computational investigation of 2D 3d/4d hexagonal transition metal borides for metal-ion batteries, Electrochimica Acta 384 (2021) 138404.
[37] Q. Liao, S. Li, F. Xi, Z. Tong, X. Chen, X. Wan, W. Ma, R. Deng, High-performance silicon carbon anodes based on value-added recycling strategy of end-of-life photovoltaic modules, Energy 128345 (2023).
[38] X. Chen, S. Wei, F. Tong, M.P. Taylor, P. Cao, Electrochemical performance of Mg-Sn alloy anodes for magnesium rechargeable battery, Electrochimica Acta 398 (2021) 139336.
[39] Y. Lu, L. Wang, J. Cheng, J.B. Goodenough, Prussian blue: a new framework of electrode materials for sodium batteries, Chemical communications 48 (2012) 6544–6546.
[40] R.Y. Wang, C.D. Wessells, R.A. Huggins, Y. Cui, Highly reversible open framework nanoscale electrodes for divalent ion batteries, Nano letters 13 (2013) 5748–5752.
[41] P. Moreau, D. Guyomard, J. Gaubicher, F. Boucher, Structure and stability of sodium intercalated phases in olivine FePO4, Chemistry of Materials 22 (2010) 4126–4128.
[42] Y. Cao, L. Xiao, M.L. Sushko, W. Wang, B. Schwenzer, J. Xiao, Z. Nie, L.V. Saraf, Z. Yang, J. Liu, Sodium ion insertion in hollow carbon nanowires for battery applications, Nano Letters 12 (2012) 3783–3787.
[43] K. Xie, W. Wei, H. Yu, M. Deng, S. Ke, X. Zeng, Z. Li, C. Shen, J.-G. Wang, B. Wei, Use of a novel layered titanoniobate as an anode material for long cycle life sodium ion batteries, RSC advances 6 (2016) 35746–35750.
[44] P. Ge, M. Fouletier, Electrochemical intercalation of sodium in graphite, Solid State Ionics 28 (1988) 1172–1175.
[45] Y. Wu, W. Wei, T. Ding, S. Chen, R. Zhai, C. Bai, Modulating a 2D heterointerface with gC 3 N 4 mesh layers: a suitable hetero-layered architecture for high-power and long-life energy storage, Journal of Materials Chemistry A 9 (2021) 7791–7806.
[46] H.-X. Zhang, P.-F. Wang, C.-G. Yao, S.-P. Chen, K.-D. Cai, F.-N. Shi, Recent advances of ferro-/piezoelectric polarization effect for dendrite-free metal anodes, Rare Metals (2023) 1–29.
[47] Y. Hwang, Y.-C. Chung, Comparative study of metal atom adsorption on free-standing h-BN and h-BN/Ni (1 1 1) surfaces, Applied surface science 299 (2014) 29–34.
[48] Y. Hwang, Y.-C. Chung, Lithium adsorption on hexagonal boron nitride nanosheet using dispersion-corrected density functional theory calculations, Japanese Journal of Applied Physics 52 (2013) 06GG08.
[49] S. Demirci, S.E. Rad, S. Kazak, S. Nezir, S. Jahangirov, Monolayer diboron dinitride: Direct band-gap semiconductor with high absorption in the visible range, Physical Review B 101 (2020) 125408.
[50] R.L. Kumawat, B. Pathak, Strong anisotropy and band Gap engineering with mechanical strains in two-dimensional orthorhombic diboron dinitride (O-B2N2), Applied Surface Science 586 (2022) 152850.
[51] S. Grimme, Accurate description of van der Waals complexes by density functional theory including empirical corrections, Journal of Computational Chemistry 25 (2004) 1463–1473.
[52] K. Adhikari, A.K. Ray, Carbon- and silicon-capped silicon carbide nanotubes: An ab initio study, Phys Lett Sect A Gen At Solid State Phys 375 (2011) 1817–1823.
[53] A.A. Peyghan, M.B. Tabar, S. Yourdkhani, A theoretical study of OH and OCH<inf>3</inf> free radical adsorption on a nanosized tube of BC<inf>2</inf>N, J. Cluster Sci. 24 (2013) 1–10.
[54] J. Du, X. Sun, G. Jiang, Structures, chemical bonding, magnetisms of small Al-doped zirconium clusters, Phys Lett Sect A Gen At Solid State Phys 374 (2010) 854–860.
[55] X. Liu, B. Zhu, Y. Gao, Structure stability of TiAu4 nanocluster with water adsorption, Phys Lett Sect A Gen At Solid State Phys 380 (2016) 1971–1975.
[56] S. Bashiri, E. Vessally, A. Bekhradnia, A. Hosseinian, L. Edjlali, Utility of extrinsic [60] fullerenes as work function type sensors for amphetamine drug detection: DFT studies, Vacuum 136 (2017) 156–162.
[57] M.W. Schmidt, K.K. Baldridge, J.A. Boatz, S.T. Elbert, M.S. Gordon, J.H. Jensen, S. Koseki, N. Matsunaga, K.A. Nguyen, S. Su, T.L. Windus, M. Dupuis, J. A. Montgomery Jr., General atomic and molecular electronic structure system, Journal of Computational Chemistry 14 (1993) 1347–1363.
[58] W. Tang, E. Sanville, G. Henkelman, A grid-based Bader analysis algorithm without lattice bias, Journal of Physics: Condensed Matter 21 (2009) 084204.
[59] G. Henkelman, B.P. Uberuaga, H. Jónsson, A climbing image nudged elastic band method for finding saddle points and minimum energy paths, The Journal of chemical physics 113 (2000) 9901–9904.
[60] Z. Zhao, T. Yu, S. Zhang, H. Xu, G. Yang, Y. Liu, Metallic P 3 C monolayer as anode for sodium-ion batteries, Journal of materials chemistry A 7 (2019) 405–411.
[61] S. Mukherjee, L. Kavalsky, C.V. Singh, Ultrahigh storage and fast diffusion of Na and K in blue phosphorene anodes, ACS applied materials & interfaces 10 (2018) 8630–8639.
[62] B. Byles, N. Palapati, A. Subramanian, E. Pomerantseva, The role of electronic and ionic conductivities in the rate performance of tunnel structured manganese oxides in Li-ion batteries, APL Materials 4 (2016) 046108.
[63] S.-Y. Chung, Y.-M. Chiang, Microscale measurements of the electrical conductivity of doped LiFePO4, Electrochemical and solid-state letters 6 (2003) A278.
[64] Y.-F. Deng, S.-X. Zhao, Y.-H. Xu, K. Gao, C.-W. Nan, Impact of P-doped in spinel LiNi0. 5Mn1. 5O4 on degree of disorder, grain morphology, and electrochemical performance, Chemistry of Materials 27 (2015) 7734–7742.
[65] C.R. Dean, A.F. Young, I. Meric, C. Lee, L. Wang, S. Sorgenfrei, K. Watanabe, T. Taniguchi, P. Kim, K.L. Shepard, Boron nitride substrates for high-quality graphene electronics, Nature nanotechnology 5 (2010) 722–726.
[66] H. Jiang, W. Shyy, M. Liu, L. Wei, M. Wu, T. Zhao, Boron phosphide monolayer as a potential anode material for alkali metal-based batteries, Journal of Materials Chemistry A 5 (2017) 672–679.
[67] X. Zhang, L. Jin, X. Dai, G. Chen, G. Liu, Two-dimensional GaN: an excellent electrode material providing fast ion diffusion and high storage capacity for Li-ion and Na-ion batteries, ACS applied materials & interfaces 10 (2018) 38978–38984.
[68] D. Er, J. Li, M. Naguib, Y. Gogotsi, V.B. Shenoy, Ti3C2 MXene as a high capacity electrode material for metal (Li, Na, K, Ca) ion batteries, ACS applied materials & interfaces 6 (2014) 11173–11179.
[69] Q. Tang, Z. Zhou, P. Shen, Are MXenes promising anode materials for Li ion batteries? Computational studies on electronic properties and Li storage capability of Ti3C2 and Ti3C2X2 (X= F, OH) monolayer, Journal of the American Chemical Society 134 (2012) 16909–16916.
[70] H. Lin, G. Liu, L. Zhu, Z. Zhang, R. Jin, Y. Huang, S. Gao, Flexible borophosphene monolayer: A potential dirac anode for high-performance non-lithium ion batteries, Applied Surface Science 544 (2021) 148895.